Sensor signal processing

Detecting Anomaly in Chemical Sensors via L1-Kernel-Based Principal Component Analysis

Hongyi Pan[1]* , Diaa Badawi[1] , Ishaan Bassi[2] , Sule Ozev[2]** , and Ahmet Enis Cetin[1]***

[1] Department of Electrical and Computer Engineering, University of Illinois Chicago, Chicago, IL 60607 USA
[2] School of Electrical, Computer, and Energy Engineering, Arizona State University, Tempe, AZ 85281 USA
* Graduate Student Member, IEEE
** Member, IEEE
*** Fellow, IEEE

Abstract—We propose a kernel-PCA-based method to detect anomaly in chemical sensors. We use temporal signals produced by chemical sensors to form vectors to perform the principal component analysis (PCA). We estimate the kernel-covariance matrix of the sensor data and compute the eigenvector corresponding to the largest eigenvalue of the covariance matrix. The anomaly can be detected by comparing the difference between the actual sensor data and the reconstructed data from the dominant eigenvector. In this letter, we introduce a new multiplication-free kernel, which is related to the ℓ_1-norm for the anomaly detection task. The ℓ_1-kernel PCA is not only computationally efficient but also energy-efficient because it does not require any actual multiplications during the kernel covariance matrix computation. Our experimental results show that our kernel-PCA method achieves a higher area under curvature score (0.7483) than the baseline regular PCA method (0.7366).

Index Terms—Sensor signal processing, sensor, ℓ_1-kernel, anomalous sensor detection, multiplication-free (MF) method, principal component analysis (PCA).

I. INTRODUCTION

Chemical sensors are widely used to detect ammonia, methane, and other volatile organic compounds (VOCs) [1], [2], [3]. The life and performance of chemical gas detection sensors can be affected by various factors, including temperature, humidity, other interfering chemical gases, physical factors, etc. Anomalous sensors can produce drifting waveforms and it is a fatal problem for reliable gas identification and concentration estimation [4], [5]. In this work, we determine anomalous sensors and sensor measurements in an array of uncalibrated sensors by using robust ℓ_1-principal component analysis (PCA) without using reference time-series data.

PCA is used in anomalous sensor and sensor signal detection [6], [7], [8]. In this approach, the covariance matrix is constructed from a set of data vectors and the anomalous items (outliers) or vectors are found by using the reconstruction difference [9], [10]. The principal components of the data covariance matrix are computed and the original data vectors are reconstructed using only the first few principal components. In general, the reconstructed data vector is similar to the original data vectors, and the reconstructed data items that are different from the corresponding original items are considered to be anomalous.

In this letter, we propose to use ℓ_1-kernel PCA based on a multiplication-free (MF) kernel to detect anomaly in chemical sensors. Although the conventional PCA, which is based on the ℓ_2-norm has successfully solved many problems, it is sensitive to outliers in the data because the effects of the outliers are overamplified by the ℓ_2-norm. Recently, it has been shown that ℓ_1-norm-based methods produce better results in practical problems compared to the ℓ_2-norm-based methods in several real-world signal, image, and video processing problems. In particular, ℓ_1-kernel PCA usually is more robust against outliers in data

compared to the ℓ_2-PCA [11]. In the ordinary ℓ_2-PCA, the principal vector is calculated as the dominant eigenvector of the data covariance matrix, which itself is calculated using the standard outer products. In this letter, we propose the eigendecomposition of the ℓ_1-kernel covariance matrix obtained using a new vector product, which induces the ℓ_1-norm without performing any multiplications. Because of low computational complexity, the ℓ_1-kernel PCA can be implemented in edge devices directly connected to the chemical sensors.

Related work includes the regular ℓ_2-PCA, kernel-PCA methods [12], the recursive ℓ_1-PCA [13], and the efficient ℓ_1-PCA via bit flipping [14]. The recursive ℓ_1-PCA [13] and the efficient ℓ_1-PCA via bit flipping [14] returns the same result while the former takes the exponential time and the latter takes the polynomial time. Both ℓ_1-PCA methods [13], [14] require some parameters to be properly adjusted and rely on recursive methods. On the contrary, the proposed ℓ_1-kernel PCA approach does not need any hyperparameter adjustments. Its implementation is as straightforward as the regular PCA because we construct a sample kernel-covariance matrix using the proposed ℓ_1-kernel and obtain the eigenvalues and eigenvectors of the kernel covariance matrix to define the linear transformation instead of solving an optimization problem.

The rest of the letter is organized as follows: In Section II, we formally introduce the ℓ_1-kernel PCA and describe its application in an anomalous chemical sensor detection task. In Section III, we compare our method with the regular PCA, the recursive ℓ_1-PCA [13], and the efficient ℓ_1-PCA via bit flipping [14]. Finally, in Section IV, we draw our main conclusions.

II. L_1-KERNEL PCA

In our recent work [11], [15], we proposed a set of kernel-based PCA methods related to the ℓ_1-norm. These Mercer-type kernels are obtained from MF dot products.
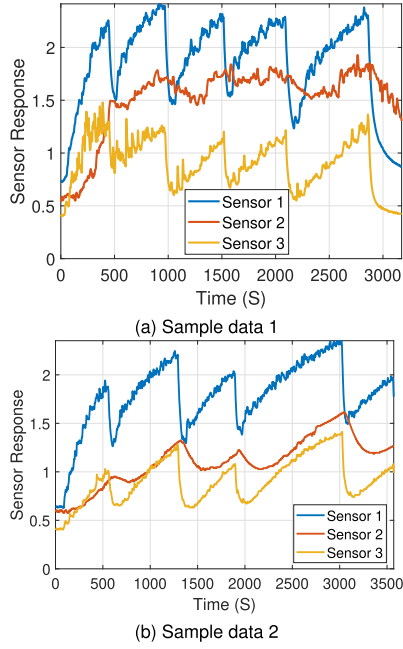
Fig. 1. Data produced by three ammonia sensors in two different ammonia gas recording experiments. The sensor 2 (in red) is the obstructed sensor. These data constitute our test set. (a) Sample data 1. (b) Sample data 2.

Let $\mathbf{w} = [w_1 \cdots w_n]^T \in \mathbb{R}^{n \times 1}$ and $\mathbf{x} = [x_1 \cdots x_n]^T \in \mathbb{R}^{n \times 1}$ be two n-dimensional column vectors. Similar to the regular dot product of vectors, we defined the MF vector product [11]. In vector data correlation operations, we use the following vector product:

$$\mathbf{w}^T \odot \mathbf{x} \triangleq \sum_{i=1}^{n} \operatorname{sign}(w_i \times x_i) \min(|w_i|, |x_i|) \qquad (1)$$

which turns out to be a Mercer type kernel: $K(\mathbf{w}, \mathbf{x}) = \mathbf{w}^T \odot \mathbf{x}$. In (1), $\operatorname{sign}(w_i \times x_i)$ can be computed without performing any actual multiplications and min operation can be implemented by subtraction and checking the sign of the result of the subtraction. For this reason, we call (1) an MF dot product. The dot product defined in (1) induces the ℓ_1-norm as $\mathbf{x}^T \odot \mathbf{x} = \sum_{i=1}^{n} \min(|x_i|, |x_i|) = \|\mathbf{x}\|_1$ and it induces a Mercer-type kernel [11].

Suppose that we collect vectors of sensor data and form a dataset $\mathbf{X} = [\mathbf{x}_1 \, \mathbf{x}_2 \, \ldots \, \mathbf{x}_D] \in \mathbb{R}^{N \times D}$. The well-known ℓ_2-PCA (regular PCA) method relies on the eigendecomposition of the sample covariance matrix $\mathbf{C} = \mathbf{X}^T \mathbf{X}$. Similarly, we estimate the kernel covariance matrix as follows:

$$\mathbf{A} = \mathbf{X}^T \odot \mathbf{X} \qquad (2)$$

where the matrix $\mathbf{A}$ is constructed using the dot products of the form $\mathbf{x}_i^T \odot \mathbf{x}_j$. As a result, the construction of the kernel-covariance matrix $\mathbf{A}$ is straightforward. We name the kernel-PCA based on the vector product in (1) as the ℓ_1-kernel PCA.

A. Anomaly Detection Using L_1-Kernel PCA

We first assume that there are D sensors and some of them are anomalous. Sensors are assumed to be close to each other and they produce correlated output waveforms, as shown in Fig. 1. We have the measurement data $\mathbf{X} = [\mathbf{x}_1 \, \mathbf{x}_2 \, \ldots \, \mathbf{x}_D] \in \mathbb{R}^{N \times D}$. The measurement data are generated by normalizing the raw sensor measurement values to $[-1, 1]$ and subtracting the mean. We construct the covariance matrix $\mathbf{A} = \mathbf{X}^T \odot \mathbf{X} \in \mathbb{R}^{D \times D}$ and calculate its eigenvectors. Let $\mathbf{v}_1 \in \mathbb{R}^{D \times 1}$ be the dominant principal component vector. Finally, we reconstruct the data segment using the vector $\mathbf{v}_1$: $\hat{\mathbf{x}}_i = \mathbf{v}_1 \mathbf{v}_1^T \mathbf{x}_i$, $i = 1, 2, .., D$ and

compute the error vector $\mathbf{x}_i - \hat{\mathbf{x}}_i$. The sensor measurement in the ith segment is assumed to be anomalous if the cumulative squared difference (CSD) between $\hat{\mathbf{x}}_i$ and $\mathbf{x}_i$ is larger than a threshold. The threshold can be set as $T = \mu + \alpha\sigma$, where μ and σ are the mean and standard deviation of CSD values learned from a training data set. The parameter α is usually selected as 3 with the Gaussianity assumption of the CSD values. If a sensor produces successive anomalous measurement vectors it is considered to be anomalous.

In the second case, we assume that we only have a single sensor. For example, the sensor 3 produces impulsive spikes between 0 and 1200 s, as shown in Fig. 1(a) (in orange). Similar to the PCA-based denoising methods [12], [16], we form data vectors from neighboring temporal data windows and form the measurement data matrix $\mathbf{X} = [\mathbf{x}_1 \, \mathbf{x}_2 \, \ldots \, \mathbf{x}_L] \in \mathbb{R}^{N \times L}$ where L is the number of data windows and we have N samples in each window. We form the kernel covariance matrix $\mathbf{A} = \mathbf{X}^T \odot \mathbf{X} \in \mathbb{R}^{L \times L}$ and compute its eigenvalues and eigenvectors $\mathbf{v}_i \in \mathbb{R}^{L \times 1}$. We reconstruct the data matrix $\hat{\mathbf{X}} = \mathbf{V}\mathbf{V}^T\mathbf{X}$ using the first l eigenvectors $\mathbf{V} = [\mathbf{v}_1, \ldots, \mathbf{v}_l]$ where $\mathbf{v}_1$ is the eigenvector corresponding to the largest eigenvalue. After this step, we compare the actual data vectors $\mathbf{x}_i$ with the reconstructed ones $\hat{\mathbf{x}}_i$, $i = 1, 2, \ldots, l$. The vectors significantly different from the reconstructed vectors are considered to be anomalous. We let $l = 1$ and observed that it is sufficient for anomaly detection.

Complexity Analysis: To calculate the covariance matrix $\mathbf{C}$, we perform $D^{2 \sim} N$ multiplications and $D^2(N - 1)$ additions because we perform N multiplications in each dot product. On the other hand, to calculate the ℓ_1-kernel covariance matrix $\mathbf{A}$, we perform $D^{2 \sim} N$ sign operations, $D^{2 \sim} N$ min operations and $D^2(N - 1)$ additions. According to [17, Table 1], a multiplication operation consumes about four times more energy compared to the MF-operations in compute-in-memory (CIM) implementation at 1 GHz operating frequency. In this letter, we have three sensors and we used an Arduino to collect data so energy efficiency will not be significant but it will be significant in a large network with its own hardware. Since the value of $D = 3$ or 5 is much smaller than the vector length $N = 125$ or 224, the eigenvector computation is negligible compared to the covariance matrix construction in this task. As a result, the ℓ_1-kernel PCA is about four times more energy efficient in CIM implementation. It is also more energy efficient in many other processors because multiplications consume more energy than additions and subtractions. [18].

Contribution: In our recent work [11], we introduced the ℓ_1-kernel PCA while this letter introduces a novel method to employ the ℓ_1-kernel PCA into the anomaly detection problem. Our experiments show that in the anomaly detection task, the ℓ_1-kernel PCA produces better results than the regular PCA, the recursive ℓ_1-PCA [13], and the efficient ℓ_1-PCA via bit flipping [14] in our dataset obtained from chemical sensors.

III. EXPERIMENTAL RESULTS

We collected data using three ammonia MQ137 Tin oxide (SnO_2)-based sensors [19]. Sensors are connected to an Arduino Uno board, and the sampling rate is 2 samples per second. Sensors and a cylindrical ammonia source are placed in an airtight chamber. Sensors are preheated for 48 h before collecting the data. When SnO_2 is heated and exposed to the air, it reacts with the oxygen present in the air and form a layer of negative ion on the surface and reduce the surface conductivity [19]. When ammonia vapor comes in contact with the surface, it combines with the oxide ion layer on the top and releases electrons for conduction. As a result, the conductivity of the surface increases. This change in surface resistance can be measured in the form of voltage. Our experimental setup is shown in Fig. 2.

Multiple Sensor Anomaly Detection: The three sensors are placed close to each other and one of the sensors (sensor 2) is obstructed by a cylindrical cover with multiple holes. The cover causes the
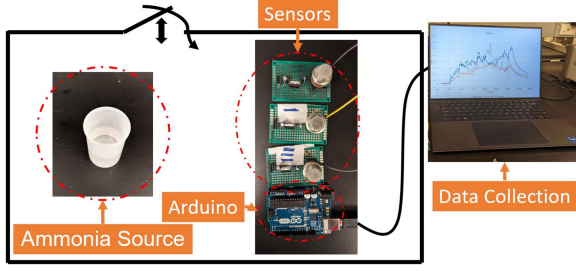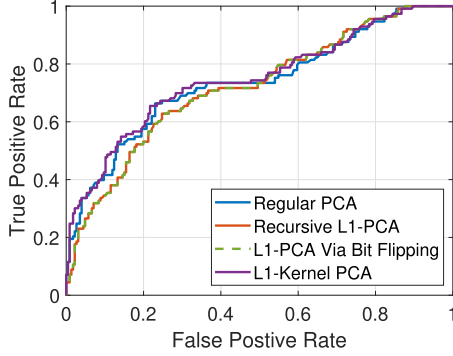
Fig. 2.   Illustration of our experimental setup.

Fig. 3.   ROC of different PCAs on the sensor data. Recursive ℓ_1-PCA [13] and ℓ_1-PCA via bit flipping [14] return the same ROC because their eigenvectors are the same.

Table 1.   AUC for Various Methods

Method	AUC score	AUC Increment
Regular PCA (baseline)	0.7366	-
Recursive ℓ_1-PCA [13]	0.7203	-0.0163
L_1-PCA via bit flipping [14]	0.7203	-0.0163
L_1-**kernel PCA**	**0.7483**	**0.0117**

The ℓ_1-kernel PCA provides the best AUC score.

sensor to react more slowly than the other sensors to the ammonia build-up and release. The obstruction level of the outlier sensor is adjusted in each trial to avoid overfitting to one condition. Moreover, to generate a more realistic environment with varying levels of ammonia concentration, the chamber lid is opened at random intervals and with random duration. Opening and closing the lid is repeated multiple times to create different rise and fall responses. Sensor waveforms from two experiments are shown in Fig. 1.

We apply the ℓ_1-kernel PCA-based anomaly detection method described in Section II-A to the data obtained from the three sensors. We compared the proposed method with the regular ℓ_2-PCA, the recursive ℓ_1-PCA [13] and the efficient ℓ_1-PCA via bit flipping [14]. The latter two compute $\mathbf{v}_1 = \arg\max_{\mathbf{v}:\|\mathbf{v}\|=1} \sum_{i=1}^{N} |\mathbf{v}^T \mathbf{x}_i|$. Tolerance parameter of the recursive ℓ_1-PCA method is set as 1×10^{-8} as suggested by Markopoulos et al. [13]. We plot the receiver operating characteristic (ROC) curve in Fig. 3 and compute the area under curve (AUC) scores for each method. As shown in Table 1 states, the ℓ_1-kernel PCA provides the highest AUC score, and the recursive ℓ_1-PCA [13] provides the lowest AUC score in this case. This is probably due to the nonconvex optimization method that they use to compute the principle vector, and the method requires a suitable tolerance parameter. On the other hand, the ℓ_1-kernel PCA does not need any tolerance parameters and the eigenvector computations are equivalent to the computational load of the regular PCA.

CSD values of the sensors' response in Fig. 1(a) using different PCAs are listed in Table 2, and CSD values of the sensors' response

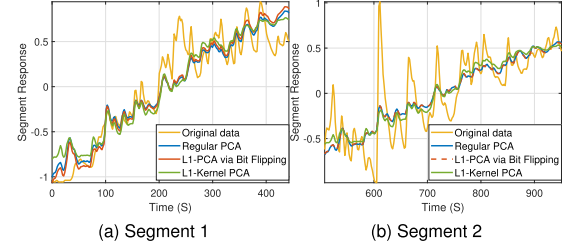(a) Segment 1   (b) Segment 2

Fig. 4.   Reconstructed waveforms of Segments 1 and 2 in Table 4. The reconstructed waveforms do not have spikes. (a) Segment 1. (b) Segment 2.

in Fig. 1(b) are listed in Table 3, respectively. The threshold values 21.63 for the regular PCA, 21.64 for the ℓ_1-PCA via bit flipping [14], and 21.61 for the ℓ_1-kernel PCA are computed from the normal cases obtained from other experiments. We have different threshold values for the regular PCA and the ℓ_1-kernel PCA because they have different principle eigenvectors. Even if we use the same threshold (21.60), the classification results in Tables 2 and 3 will not change.

Sensor 2 does not always exhibit anomalous behavior. In general, its response increases due to ammonia gas exposure but does not decrease as fast as the other sensors when there is no gas, as shown in Fig. 1. The regular PCA detects the anomalous behavior of Sensor 2 in 9 out of 28 data segments. On the other hand, the ℓ_1-PCA via bit flipping and our ℓ_1-kernel PCA detect the anomalous behavior of Sensor 2 in 10 out of 28 data segments. Moreover, the regular PCA and the ℓ_1-PCA via bit flipping produce a false alarm in the second data segment (250–499 s) of Sensor 1 as shown in Table 3 while our ℓ_1-kernel PCA avoids this false alarm case. In conclusion, ℓ_1-kernel PCA produces better results than the regular PCA, the recursive ℓ_1-PCA [13] and ℓ_1-PCA via bit flipping [14].

Anomaly Detection Using a Single Sensor: During the first three ammonia gas exposures, the sensor 3 positively responds but it also produces spikes up to 1200 s, as shown in Fig. 1(a). Multisensor PCA-based anomaly detection cannot detect this behavior because only the sensor 1 works properly before 1200 s. However, we compare the current sensor window of Sensor 2 with its neighboring data windows, we can identify the anomalous behavior. We used $L = 5$ data segments to construct the 5×5 covariance and ℓ_1-kernel covariance matrices. In each data segment, we have $N = 224$ measurement. We used only the dominant eigenvector to estimate the data segments.

The regular PCA, the ℓ_1-PCA via bit flipping, and the ℓ_1-kernel PCA reconstructed waveforms do not have spikes and that is how we can identify the anomaly in sensor readings, as shown in Fig. 4. Table 4 shows the CSD values of these methods and they correctly identified the anomolous segments.

IV. CONCLUSION

In this letter, we presented a framework for detecting anomalous sensors and sensor measurements in a chemical sensory system using the ℓ_1-kernel PCA. We collected data from three commercial Tin Oxide (SnO$_2$) sensors by exposing them to ammonia in an environment-controlled experiment. The proposed ℓ_1-kernel PCA is more robust than the regular PCA in our experiments. This is due to the fact that ℓ_1-kernel PCA is related with the ℓ_1-norm and it gives less emphasis to anomalous spikes in sensor measurements while computing the correlation matrix. The computational energy cost of the ℓ_1-kernel PCA is much lower than the regular PCA on many processors. Because of low energy complexity, the ℓ_1-kernel PCA can be implemented in low-cost edge devices directly connected to the chemical sensors.

Table 2. CSDs of the Sample Data 1 in Fig. 1(a) Using Regular PCA

Segment (Time/S)	Regular PCA			L_1-PCA via Bit Flipping [14]			L_1-Kernel PCA		
	Sensor 1	Sensor 2	Sensor 3	Sensor 1	Sensor 2	Sensor 3	Sensor 1	Sensor 2	Sensor 3
0–249	7.54	9.44	2.20	8.12	9.01	2.37	8.01	9.08	2.21
250–499	**25.61**	18.48	9.23	**21.82**	**23.66**	8.71	19.54	**27.64**	7.24
500–749	11.81	12.19	17.13	16.46	9.23	16.57	14.06	10.96	16.59
750–999	0.71	**24.75**	1.08	0.76	**25.86**	0.85	0.75	**25.26**	0.90
1000–1249	3.03	9.11	11.88	2.93	9.04	12.08	3.14	8.70	12.35
1250–1499	4.57	7.02	1.30	6.03	6.48	1.89	4.64	6.92	1.38
1500–1749	5.71	**31.50**	2.79	10.60	**30.41**	1.16	7.84	**30.97**	1.73
1750–1999	3.77	**28.11**	3.52	1.31	**40.71**	0.87	3.32	**29.27**	3.01
2000–2249	1.29	14.74	2.04	1.13	15.34	1.83	1.46	14.61	2.13
2250–2499	2.09	**26.11**	3.55	1.94	**25.57**	5.40	1.98	**25.95**	3.88
2500–2749	5.08	6.08	7.39	5.13	5.53	8.61	4.95	6.32	7.37
2750–2999	1.09	10.67	1.87	1.05	10.91	1.77	1.17	10.66	1.86
3000–3249	0.98	12.89	3.51	0.92	13.22	3.30	0.99	12.94	3.51

Sensor 2 is obstructed. Values larger than threshold 21.60 are in bold.

Table 3. CSDs of the Sample Data 2 in Fig. 1(b) Using Regular PCA

Segment (Time/S)	Regular PCA			L_1-PCA via Bit Flipping [14]			L_1-Kernel PCA		
	Sensor 1	Sensor 2	Sensor 3	Sensor 1	Sensor 2	Sensor 3	Sensor 1	Sensor 2	Sensor 3
0–249	1.82	11.52	1.32	2.04	11.31	1.43	2.09	11.29	1.45
250–499	2.55	1.30	1.06	2.52	1.35	1.10	2.52	1.35	1.06
500–749	13.63	11.07	6.61	13.97	11.38	6.19	13.55	10.91	6.93
750–999	4.62	6.93	1.36	4.63	6.90	1.41	4.37	7.42	1.25
1000–1249	3.28	1.76	1.85	3.22	1.77	2.01	3.25	1.81	1.86
1250–1499	4.76	**50.56**	1.51	3.67	**52.57**	1.21	5.12	**50.12**	1.92
1500–1749	1.68	**28.23**	0.92	2.03	**27.83**	1.08	2.10	**27.71**	1.20
1750–1999	0.98	21.09	3.91	0.98	21.09	3.92	1.22	20.74	4.20
2000–2249	2.65	18.01	18.88	2.83	17.34	19.43	2.41	20.60	17.05
2250–2499	5.67	4.72	1.41	5.67	4.73	1.40	5.52	4.95	1.39
2500–2749	3.62	1.58	0.61	3.58	1.63	0.63	3.57	1.65	0.62
2750–2999	1.97	1.55	1.81	1.96	1.58	1.79	1.98	1.61	1.78
3000–3249	5.54	**50.49**	1.79	3.67	**54.51**	0.92	5.72	**50.23**	1.99
3250–3499	3.58	**37.25**	1.29	4.62	**35.78**	1.93	3.13	**38.00**	1.06
3500–3749	2.53	**35.25**	4.93	1.23	**40.35**	3.07	2.42	**35.53**	4.78

Sensor 2 is obstructed. Values larger than threshold 21.60 are in bold.

Table 4. CSD Values Due to Ammonia Exposure of Sensor 3

Segment	Regular PCA	L_1-PCA via Bit Flipping	L_1-Kernel PCA
1	**9.62**	**9.51**	**9.79**
2	**13.59**	**13.64**	**13.55**
3	**7.21**	**7.30**	**7.26**
4	4.35	4.58	4.38
5	3.48	3.62	3.65

The first three segments contain impulsive spikes.

ACKNOWLEDGEMENT

REFERENCES

[1] A. Vergara, S. Vembu, T. Ayhan, M. A. Ryan, M. L. Homer, and R. Huerta, "Chemical gas sensor drift compensation using classifier ensembles," *Sensors Actuators B: Chem.*, vol. 166, pp. 320–329, 2012.

[2] F. Erden, E. B. Soyer, B. U. Toreyin, and A. E. Cetin, "VOC gas leak detection using Pyro-electric infrared sensors," in *Proc. IEEE Int. Conf. Acoust., Speech, Signal Process.*, 2010, pp. 1682–1685.

[3] D. Badawi, H. Pan, S. C. Cetin, and A. E. Çetin, "Computationally efficient spatio-temporal dynamic texture recognition for volatile organic compound (VOC) leakage detection in industrial plants," *IEEE J. Sel. Topics Signal Process.*, vol. 14, no. 4, pp. 676–687, May 2020.

[4] Fahim, Mainuddin, U. Mittal, J. Kumar, A. T. Nimal, and M. U. Sharma, "Single chip readout electronics for saw based gas sensor systems," in *Proc. IEEE Sensors*, 2017, pp. 1–3.

[5] E. H. Egilmez and A. Ortega, "Spectral anomaly detection using graph-based filtering for wireless sensor networks," in *Proc. IEEE Int. Conf. Acoust., Speech, Signal Process.*, 2014, pp. 1085–1089.

[6] L. Huang, X. L. Nguyen, M. Garofalakis, M. I. Jordan, A. Joseph, and N. Taft, "In-network PCA and anomaly detection," in *Proc. Adv. Neural Inf. Process. Syst.*, 2006, pp. 617–624.

[7] V. Chatzigiannakis and S. Papavassiliou, "Diagnosing anomalies and identifying faulty nodes in sensor networks," *IEEE Sensors J.*, vol. 7, no. 5, pp. 637–645, May 2007.

[8] L. Erhan et al., "Smart anomaly detection in sensor systems: A multi-perspective review," *Inf. Fusion*, vol. 67, pp. 64–79, 2021.

[9] Y. Yao, A. Sharma, L. Golubchik, and R. Govindan, "Online anomaly detection for sensor systems: A simple and efficient approach," *Perform. Eval.*, vol. 67, no. 11, pp. 1059–1075, 2010.

[10] A. Sree and K. Venkata, "Anomaly detection using principal component analysis," *J. Comput. Sci. Technol.*, vol. 5, no. 4, pp. 124–126, 2014.

[11] H. Pan, D. Badawi, E. Koyuncu, and A. E. Cetin, "Robust principal component analysis using a novel kernel related with the ℓ_1-norm," in *Proc. 29th Eur. Signal Process. Conf.*, 2021, pp. 2189–2193.

[12] B. Schölkopf, A. Smola, and K. Müller, "Kernel principal component analysis," in *Proc. Int. Conf. Artif. Neural Netw.*, 1997, pp. 583–588.

[13] P. P. Markopoulos, G. N. Karystinos, and D. A. Pados, "Optimal algorithms for l_1-subspace signal processing," *IEEE Trans. Signal Process.*, vol. 62, no. 19, pp. 5046–5058, Oct. 2014.

[14] P. P. Markopoulos, S. Kundu, S. Chamadia, and D. A. Pados, "Efficient l1-norm principal-component analysis via bit flipping," *IEEE Trans. Signal Process.*, vol. 65, no. 16, pp. 4252–4264, Aug. 2017.

[15] C. E. Akbaş, O. Günay, K. Taşdemir, and A. E. Çetin, "Energy efficient cosine similarity measures according to a convex cost function," *Signal, Image, Video Process.*, vol. 11, no. 2, pp. 349–356, 2017.

[16] S. B. Mike, B. Scholkopf, and A. J. Smola, "Kernel PCA and denoising in feature space," in *Proc. Adv. Neural Inf. Process. Syst.*, 1999, pp. 524–536.

[17] S. Nasrin et al., "ENOS: Energy-aware network operator search for hybrid digital and compute-in-memory DNN accelerators," 2021, *arXiv:2104.05217*.

[18] S. Nasrin, D. Badawi, A. E. Cetin, W. Gomes, and A. R. Trivedi, "MF-Net: Compute-in-memory SRAM for multibit precision inference using memory-immersed data conversion and multiplication-free operators," *IEEE Trans. Circuits Syst. I: Reg. Papers*, vol. 68, no. 5, pp. 1966–1978, May 2021.

[19] J. Watson, K. Ihokura, and G. S. V. Coles, "The tin dioxide gas sensor," *Meas. Sci. Technol.*, vol. 4, no. 7, 1993, Art. no. 711.